Catalysis Today 423 (2023) 113952

Contents lists available at ScienceDirect

Catalysis Today

journal homepage: www.elsevier.com/locate/cattod

Development of nickel catalysts supported on silica for green diesel production

John Zafeiropoulos [a], George Petropoulos [a], Eleana Kordouli [a,b,c], Christos Kordulis [b,c], Alexis Lycourghiotis [a,b], Kyriakos Bourikas [a,*]

[a] School of Science and Technology, Hellenic Open University, Parodos Aristotelous 18, GR-26335 Patras, Greece
[b] Department of Chemistry, University of Patras, GR-26504 Patras, Greece
[c] Foundation of Research and Technology – Institute of Chemical Engineering Science (FORTH/ICE-HT), Stadiou Str. Platani, P.O. Box 1414, GR-26500 Patras, Greece

ARTICLE INFO

Keywords:
Silica
Green diesel
Nickel catalysts
Biofuels
Selective deoxygenation
Renewable diesel

ABSTRACT

Two series of nickel catalysts supported on silica were prepared and evaluated for the selective deoxygenation of sunflower oil into green diesel, under conditions without solvent. The catalysts were characterized with various techniques (N_2 physisorption, CO chemisorption, XRD, SEM-EDS, TEM, H_2-TPR, NH_3-TPD). The first series involves catalysts with Ni content ranging between 10 and 60 wt%, synthesized by successive dry impregnation. The green diesel in the liquid product seems to depend mainly on the active nickel surface and the moderate acidity, following a volcano trend which is maximized over the sample with 50 wt% Ni loading. The second series concerns catalysts with 50 wt% Ni, synthesized by the use of four different techniques: Successive Dry Impregnation (SDI), Wet Impregnation (WI), using $Ni(en)_3(NO_3)_2$ (en: ethylene diamine) as the Ni precursor and Deposition – Precipitation at room temperature (DP-NH_3), Deposition – Precipitation at high temperature (DP-Urea), using $Ni(NO_3)_2$ as the Ni precursor. SDI or WI results mainly to granular nickel supported nanoparticles, whereas DP-NH_3 and mainly DP-Urea to the formation of filamentous structures of a nickel phyllosilicate phase. The performance of the catalysts towards the production of green diesel follows the order WI>SDI> DP-NH_3 >DP-Urea. The catalyst synthesized by WI exhibits the higher active surface in combination with high population of sites of moderate acidity. The catalysts prepared by DP, although exhibiting a very high surface area and a very high nickel dispersion, did not appear more effective in the n-alkanes production, due to the formation of a very well dispersed nickel phyllosilicate phase, but not fully reducible even at very high temperatures and thus inactive in the selective deoxygenation of sunflower oil.

1. Introduction

Our planet is facing an energy and mainly environmental crisis due to the widespread use of fossil fuels. Their replacement by renewable energy sources, including biomass, seems to be a promising solution [1]. Biofuels produced form the latter is indeed a good alternative, reducing also geographical inequality in energy production.

Vegetable oils, micro-algal oils, waste cooking oils and animal fats constitute a very attractive category of biomass since the ratios of oxygen to carbon and hydrogen atoms in their triglyceride molecules are lower compared with those in other categories of biomass (e.g., bio-oil from lignocellulosic biomass). In fact, the carbon chains of triglyceride biomass are similar to the hydrocarbons contained in the petroleum fractions [2].

However, natural triglycerides cannot be used directly as transportation fuels. They should be upgraded. The most common way is to convert them, via transesterification, to fatty acid methyl esters, so-called biodiesel [3]. However, there are important problems associated with the production, storage and use of biodiesel, which limit its content (<20%) in blends with petro-diesel [4]. These problems encourage intensive research to find alternative methods of upgrading natural triglycerides. A promising relatively new technology is the Selective Deoxygenation (SDO) of natural triglycerides [5–7]. This process can effectively remove oxygen without fragmentation of the side chains of triglycerides. It takes place at moderate temperatures (240–360°C) and relatively high hydrogen pressures (10–80 bar), through three different pathways, namely decarboxylation (deCO_2), decarbonylation (deCO) and hydrodeoxygenation (HDO) reactions (Scheme 1). Thus,

* Corresponding author.
E-mail address: bourikas@eap.gr (K. Bourikas).

https://doi.org/10.1016/j.cattod.2022.11.013
Received 28 March 2022; Received in revised form 22 September 2022; Accepted 5 November 2022
Available online 8 November 2022

n-alkanes in the diesel range (C15–C18) can be produced. This product is the so-called green or renewable diesel.

Concerning the mechanism of the above reaction scheme, deCO$_2$ proceeds through decarboxylation of the intermediate fatty acids, deCO proceeds through decarbonylation of the intermediate fatty aldehydes and HDO proceeds through dehydration of the intermediate fatty alcohols followed by hydrogenation of the resulting alkenes [6,8].

The industrial production of green diesel, by hydrotreatment of natural triglycerides via SDO, can be realized mainly through two different approaches: the co-process with petroleum fractions [9] and the stand-alone process [10]. In the second one, some noble metal supported catalysts [11–15], as well as conventional sulfide NiMo, CoMo and NiW supported catalysts [16–18], appear to be very reactive and selective. However, the economic viability of the noble metal catalysts is doubtful. On the other hand, the need of conservation of the sulfide form of the conventional NiMo, CoMo and NiW catalysts impose the introduction of a sulfur compound into the feed. Unfortunately, this increases the complexity of the process and the probability of a sulfur-contaminated end product [19,20].

In view of the above, the research effort was progressively shifted to the development of cheaper and efficient non-sulphided nickel-based catalysts [19], acting mainly in their reduced state [8]. The research development, reviewed by our group [8] as well as other groups [6,21], continues intensively up today. It has been proved that nickel catalysts accelerate mainly the decarbonylation/decarboxylation (deCOx) of intermediate aldehydes (being in equilibrium with fatty alcohols) and fatty acids, respectively.

Two crucial factors determine the SDO activity and selectivity of the metallic nickel catalysts. The first is the high nickel content in combination with high specific surface area, so that the supported catalyst to exhibit high nickel active surface. The second crucial factor is the choice of the support. Various supports have been studied concerning the selective deoxygenation of fatty compounds [6,22–25]. The support should exhibit high surface area for the good dispersion of nickel nanoparticles and mild acidity for both promoting SDO and preventing extensive cracking [8]. Silica seems a promising support since it meets these conditions and thus it is our choice in the present work. Nickel supported on silica catalysts have been reported in the literature [26–39], most of them in the metallic or phosphide form. The survey of the literature showed that in almost all studies the catalysts had Ni loading up to 25%. Thus, relatively low Ni loadings have been used since today. On the other hand, most of the catalysts have been prepared through simple techniques such as wet [26,29–31,33–36,38,39] or dry impregnation [27,28,37] and only one through a non-conventional method (namely through impregnation-chemical reduction [32]). Moreover, as far as we know from the literature, there are no studies dealing with the influence of the synthesis method of Ni/SiO$_2$ catalysts on their efficiency for the transformation of fatty compounds to fuels.

In view of the above, in the present work we attempt a detailed study of SDO of natural triglycerides over nickel supported on silica catalysts, aiming to obtain a clear picture about the optimum Ni loading as well as the optimum preparation route. The study was implemented in two stages. In the first stage, we studied a series of nickel catalysts with Ni loading in the range 0–60 wt% Ni. The scope of this stage was to find out the optimum catalyst composition. Adopting this composition, in the second stage, we examined the effect of preparation technique on the physicochemical characteristics and catalytic activity. Four preparation methodologies have been adopted: the successive dry impregnation, the wet impregnation, the deposition – precipitation at room temperature and the deposition – precipitation at high temperature.

In the first two methodologies, Ni(en)$_3$(NO$_3$)$_2$ (en: ethylene diamine) has been chosen as the Ni precursor, since it has been shown in the literature that the use of this kind of precursors (chelated metal complexes) in silica supported catalysts results in catalysts with high dispersion and desired physicochemical characteristics [40–46]. More specifically, Negrier et al. [47] studying the role of ethylenediamine in the preparation of alumina-supported Ni catalysts, applied a protocol where the dried samples were subjected to thermal treatment in Ar. This led to a complete auto reduction of the complexes and the formation of very well dispersed Ni^0. Later on, the same group [48,49] suggested a post-treatment in hydrogen as necessary both to remove carbonaceous deposits and to fully reduce nickel ions into the metallic state. However, when the same research group synthesized Ni/SiO$_2$ catalysts through grafting of the ethylenediamine comlex of Ni on silica [44], they performed a calcination step before reduction. They found that this step transforms these complexes into isolated Ni^{2+} ions, which are reduced into small metallic Ni particles with a homogeneous size distribution, even at high Ni loadings. Thus, this protocol was also followed by us in the present study, in order to maximize the metallic nickel surface on the catalysts.

Deposition – precipitation, using Ni(NO$_3$)$_2$ × 6 H$_2$O as nickel precursor, was, moreover, adopted since it is well-known that allows mounting a large amount of active phase on the support, keeping low its particle size (high dispersion) [50–52]. In addition, we have contributed to this area by developing either a co-precipitation methodology or a deposition – precipitation one, achieving a severe control of the synthesis parameters. This allowed us to prepare nickel/alumina [53,54] nickel/zirconia [55] and nickel/palygorskite [56] catalysts with high surface area even for catalysts containing very high nickel content.

The catalysts were characterized with various techniques and evaluated in the SDO of sunflower oil (SFO) in a high pressure semi-batch reactor. Two significant differences of the present contribution in relation to the majority reported in the literature should be mentioned: the first is that the evaluation of the catalysts took place in conditions free of solvent, and the second is the very large amount of oil (100 mL) in proportion to that of the catalyst (1 g) in combination with the reaction time (9 h). These conditions are equivalent to an LHSV value of 11.1 h^{-1}, for a corresponding study in a fixed bed reactor. They are very hard in comparison to the corresponding ones reported in previous relative studies. SFO as feedstock was chosen because of the following reasons: (a) SFO is widely used in many countries as a raw material for biodiesel production. So in the context of renewable energy policies, an SFO-based process is attractive and cost-effective, (b) SFO may be an edible oil, but genetically modified sunflower grown on barren land (e.g. old mining lands, irrigation canals) is considered a viable source of biofuels because it does not compete with arable land [57] and (c) sunflower seeds have high oil content (about 50%). Taking into account all the above, as well as the fact that the green diesel production is economically advantageous or of equal cost compared to the biodiesel production [58–60], one can claim that SFO will be used in the near future for the production of green diesel. As for the amount of SFO available, it is a fact that it is not enough to replace the entire amount of

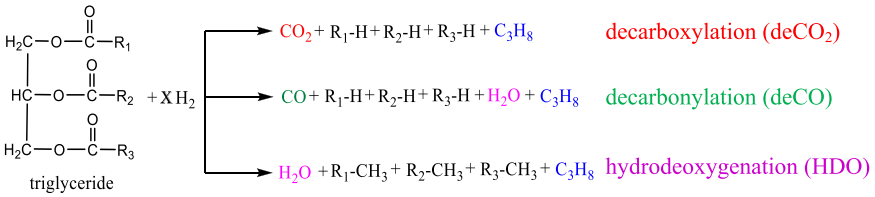

Scheme 1. The reactions involved in the process of the Selective DeOxygenation (SDO).

diesel used today. This of course applies to all vegetable, algal and waste cooking oils. However, the prospect of even partial replacement of diesel from renewable diesel is possible, and very likely, given both environmental constraints on the one hand and the evolution of agricultural technology on the other. For example, the genetically modified sunflower plants mentioned earlier are characterized by low moisture and fertility requirements, and thus can grow even in barren soil [57].

2. Experimental

2.1. Reagents and materials

For the synthesis of the catalysts through various techniques, we used the following reagents: nickel nitrate ($Ni(NO_3)_2 \times 6\ H_2O$, Alpha Aesar), urea ($(NH_2)_2CO$, Duchefa Biochemie), ammonium hydroxide solution (NH_4OH 30%, Riedel-de Haen), ethylenediamine (Sigma – Aldrich), acetone (Sigma –Aldrich) and triple distilled water. SiO_2 (Alfa, amorphous fumed, 99.8% metal base 325 mesh) was used as support. Sunflower oil (purchased from the local market) was used as a feedstock for the reaction. Details concerning its composition and physicochemical characteristics have been previously reported [61].

2.2. Synthesis of the precursor solid $Ni(en)_3(NO_3)_2$

The synthesis of the precursor solid $Ni(en)_3(NO_3)_2$ (en: ethylene diamine) was performed in the lab, according to the following procedure. A weighed amount of nickel nitrate (14.54 g) was placed in a 100 mL beaker and then 10 mL of triple distilled water were added in it, under continuous stirring. After the dissolution of the solid, the beaker was placed in an ice bath, so that the temperature can be maintained between 2 and 10 °C, as the complexation reaction is strongly exothermic. After the solution has stabilized at the desired temperature and under constant stirring, we start adding the ethylene diamine (11 mL) at such a rate as to keep the temperature between 2 and 10 °C. The complex begins to form when, from the characteristic green color that the solution has at the beginning, it acquires a purple color. After adding all of the ethylene diamine, the solution was left to equilibrate and then was filtered through a 0.22 μm filter to recover the solid complex, which is then washed with 6 mL of acetone. After recovering the complex, we place it for drying in the oven at 50 °C for 24 h. The yield we achieved was close to 70%.

2.3. Synthesis of the catalysts

2.3.1. Successive Dry Impregnation (SDI)

The SDI catalysts were synthesized using successive dry impregnation of the silica support with aqueous solution having volume equal to the support pore volume (0.54 $cm^3\ g^{-1}$). The solution was prepared by dissolving a given amount of the precursor solid $Ni(en)_3(NO_3)_2$ in an ammonium nitrate solution (0.1 M). The precursor had been previously synthesized in the laboratory. The need for using successive dry impregnations instead of one impregnation step was due to the minimum volume required for the impregnating solution which was determined by the $Ni(en)_3(NO_3)_2$ solubility and the high Ni loading of the catalysts. Details about the quantities of support, nickel precursor and impregnation solution used for the synthesis of each catalyst are given in Table 1. After each impregnation step (the number of which depends on the final Ni loading of the sample) the sample was dried at 120 °C for 30 min in order the solvent to be removed and the next impregnation step to take place. Each final solid was dried at 110 °C for 24 h and calcined at 400 °C for 2 h.

2.3.2. Wet impregnation (WI)

Following wet impregnation, 1.5 g of SiO_2 and 50 mL of the impregnating solution of the precursor salt (9.28 g $Ni(en)_3(NO_3)_2$) were placed in a spherical flask of a rotary evaporator, followed by the addition of 50 mL ammonium nitrate solution (0.1 M). The suspension was left under rotation, at temperature 90 °C and pressure 500 mbar till evaporation of the solvent. The obtained solid was dried at 110 °C for 24 h and calcined at 400 °C for 2 h.

Table 1
Quantities of support, nickel precursor, impregnation solution and number of impregnations used for the synthesis of the catalysts through the SDI technique (xNiSi SDI, where x denotes the wt% loading).

Catalyst	SiO_2 (g)	Ni $(en)_3(NO_3)_2$ (g)	Volume of impregnation solution (mL)	Number of impregnations
10NiSi SDI	2.7	1.86	1.5	1
20NiSi SDI	2.4	3.71	3	3
30NiSi SDI	2.1	5.57	4.5	5
40NiSi SDI	1.8	7.42	6	7
50NiSi SDI	1.5	9.28	7.5	10
60NiSi SDI	1.2	11.23	9	14

2.3.3. Deposition precipitation at room temperature (DP-NH_3)

Catalyst synthesis by Deposition Precipitation at room temperature took place in a thermostatic vessel placed on magnetic stirrer. The experimental set up includes a pH control system and a dosimat (836 Titrando, Metrohm). SiO_2 powder and $Ni(NO_3)_2 \times 6\ H_2O$, as the metal precursor salt, were used. The pH control system allowed the automatic adjustment of the pH during the synthesis, by adding to the vessel drops of 10% v/v aqueous solution of NH_4OH. N_2 was pumped into the vessel to prevent the dilution of the atmospheric CO_2. For the synthesis of the catalyst, 1.5 g of SiO_2 powder and 100 mL of triple distilled water were added into the thermostatic vessel under stirring at 25 °C. 7.43 g of Ni $(NO_3)_2 \times 6\ H_2O$ were dissolved in 100 mL of triple distilled water and were placed in the first burette of the system. The pH was adjusted at a value equal to 7.5 and the dosimat was adding the nickel nitrate solution to the vessel with a rate of 0.5 mL/min. As pH was decreasing due to the deposition – precipitation of the $\left[Ni(H_2O)_6\right]^{2+}$ ions, the pH control system was feeding the solution with drops of the NH_4OH solution (through the second burette) so that pH was kept at its initial value. When the system stopped to feed NH_4OH solution, the deposition-precipitation process had reached the end and thus the suspension was filtered. The obtained solid was dried at 110 °C for 24 h and calcined at 400 °C for 2 h.

2.3.4. Deposition precipitation at high temperature (DP-Urea)

For the deposition precipitation method at high temperature, 7.43 g of $Ni(NO_3)_2 \times 6\ H_2O$ was dissolved in 100 mL of triple distilled water in a spherical flask (250 mL) and then 1.5 g of silica powder was added. Next, 100 mL of $CO(NH_2)_2$ aqueous solution were added. The final concentration of urea was triple to that of the NO_3^- ions from the nickel salt. The suspension was equilibrated for 1 h on a magnetic stirrer and under a reflux condenser. Then, the flask was heated in an oil bath at 110 °C for 10 h. After that period the suspension was cooled to ambient temperature and filtered under vacuum. The obtained solid was dried at 110 °C for 24 h and calcined at 400 °C for 2 h.

2.4. Activation of the catalysts

The calcined samples obtained in all cases using various synthesis methods (as described above) were heated in a fixed bed reactor with a rate of 10 °C/min up to 400 °C, under Ar flow (30 mL/min) and then were reduced at that temperature for 2.5 h, under H_2 flow (40 mL/min). Activation was followed by passivation, by feeding the reactor with 1%

v/v O_2 in Ar stream (20 mL/min) for half an hour, at room temperature. The final catalysts are symbolized as xNiSi-y, where x stands for the nickel loading (wt% Ni) and y for the preparation method (y: SDI, WI, DP-NH_3, DP-Urea).

2.5. Characterization of the catalysts

2.5.1. Determination of surface area and porosity

Surface area and porosity measurements took place in a Micromeritics apparatus (Tristar 3000 porosimeter). The calculation of specific surface area (S_{BET}) was based on BET equation and the pore size distribution was determined using the BJH method.

2.5.2. Transmittance electron microscopy (TEM)

TEM was used for recording images of the catalysts and determine the mean nickel particle size in a JEOL JEM-2100 system operated at 200 kV (resolution: point 0.23 nm, lattice 0.14 nm) equipped with an Erlangshen CCD Camera (Gatan, Model 782 ES500W). The specimens were prepared by dispersion in water and spread onto a carbon-coated copper grid (200 meshes).

2.5.3. X-ray diffraction (XRD)

X-ray diffraction patterns (in the range $10^\circ \leq 2\theta \leq 80^\circ$) were recorded in a Bruker D8 Advance diffractometer, equipped with a nickel-filtered CuKα (1.5418 Å) radiation source, working at 40 kV and 40 mA. The step size and the time per step values were equal to 0.02° and 0.5 s, respectively. The mean crystallite size was determined by applying Scherrer's equation.

2.5.4. Temperature programmed reduction with H_2 (H_2-TPR)

H_2-TPR experiments were performed for the characterization of the precursor samples (before reduction and after Ar treatment at 400 °C) in a lab-made apparatus. 0.04 g of the sample was placed in a quartz microreactor. Then, a reducing gas mixture (H_2/Ar: 5/95 v/v) was passed for 2 h, with a flow rate of 40 mL/min, at room temperature. After that, the temperature was increased to 1000 °C with a rate of 10 °C/min. The hydrogen concentration of the gas mixture at the exit was determined by using a thermal conductivity detector (TCD), after the gas mixture had been dried in a cold trap (−95 °C).

2.5.5. Temperature programmed desorption of ammonia (NH_3-TPD)

NH_3-TPD experiments were conducted in the same apparatus, as previously, for the determination of the acidity of the catalysts. 100 mg of the reduced sample was placed in the quartz microreactor. Then, He was passed with flow rate of 30 mL/min, for 30 min, in order any adsorbed species to be removed from the sample surface. Subsequently, a stream of NH_3 was passed in the microreactor for 30 min at room temperature and then it was switched to He in order the physically adsorbed NH_3 to be removed. Then, the temperature was increased up to 600 °C with a rate of 10 °C/min. The quantity of the desorbed ammonia was determined by the use of the TCD.

2.5.6. CO chemisorption

CO-chemisorption was performed on a laboratory constructed apparatus consisted of a gas handling system (Brooks, Read Out & Control Electronics and mass flow controllers 58505 S), a quartz U shape fixed bed microreactor, a tubular furnace and a TCD detector (Shimadzu GC-2014), following pulse technique. More precisely, the synthesized samples, after calcination, were placed in the microreactor and pre-treated at 400 °C under Ar flow (30 mL/min) for 1 h to clean the surface of the oxidic precursors. Then, ~150 mg of the oxidic precursor sample was activated by in – situ reduction at 400 °C for 2.5 h under hydrogen flow (30 mL/min). After activation, the system was cooled down to room temperature under He flow (30 mL/min), until a constant base line to be seen on the TCD detector. The CO uptake was measured at 25 °C by successive injection of 0.5 mL of CO (10 v/v % in He) pulses via a calibrated loop of a six-port valve into He carrier until saturation peak was obtained. Subsequently, the catalyst surface was washed with He for 0.5 h and another cycle of successive injections was performed. The chemically adsorbed CO was determined by subtracting the CO adsorbed during the second cycle from that of the first one.

2.5.7. Scanning electron microscopy - energy dispersive spectrometry (SEM-EDS)

SEM-EDS was used to obtain microphotographs of the catalysts and to confirm the percentage amount of nickel in the catalysts. A Scanning Electron Microscope (SEMJEOL JSM6300) together with an Energy Dispersive Spectrometry accessory have been used. It was working with 20 kV accelerating voltage and 10 nA beam current. Microanalysis was performed on gold coated samples, which were mounted directly on the sample holder.

2.6. Evaluation of the catalysts

The evaluation of the catalysts performance in the transformation of sunflower oil to green diesel, through hydrotreatment, took place in a semi-batch reactor (300 mL, Autoclave Engineers) without solvent. The reaction conditions were the following: temperature 310 °C, hydrogen pressure 40 bar, oil volume to catalyst mass 100 mL / 1 g and stirring speed 2000 rpm. After the addition of both the catalyst and the oil, the reactor was heated with a rate of 10 °C/min at the desired reaction temperature, under Ar flow (100 mL/min) to purge the dead volume from the ambient air. After that, the Ar stream was changed to H_2 with the same flow rate and the hydrogen pressure was maintained constant at 40 bar, during the 9 h experiment. The reaction was monitored for the whole period by collecting liquid samples from the reactor every hour. The samples were analyzed in a gas chromatograph (Shimadzu GC-2010 plus) equipped with a flame ionization detector (FID) and an appropriate column (ZB-5HT, INFERNO, ZEBRON, l=30 m, d=0.52 mm, tf=0.10 μm), working in a split mode (split ratio: 40). The temperature pattern adopted for the analysis was the following: 50∘C for 2.5 min, increase up to 180∘C with a rate of 10∘C/min, 180∘C for 1 min, increase up to 230∘C with a rate of 7∘C/min, 230∘C for 1 min, increase up to 390∘C with a rate of 14∘C/min, 390∘C for 6 min. The injector and detector temperatures were 350 °C and 420 °C, respectively. Heptane (Sigma-Aldrich, ≥ 99% n-heptane basis) was used for dilution (1:20) of the liquid samples taken from the reactor and as external standard for quantification of the results. The various products of the liquid samples were identified with a gas chromatography − mass spectrometry system (Shimadzu GCMS-QP2010 Ultra).

3. Results and discussion

3.1. Catalysts' characterization

Textural characterization of the catalysts was performed by the use of N_2 physisorption technique at liquid N_2 temperature. The N_2 adsorption–desorption isotherms (not shown), obtained for the catalysts of the first series (xNiSi SDI, where x denotes the wt% loading), exhibit adsorption isotherms of type IV with the H1 hysteresis loop, which is typical of mesoporous materials. Pore size distribution curves (Fig. 1(A)) proved that the majority of pores in all cases belongs to mesoporous range (1.7 – 50 nm) and that there is also a fraction of small macropores (> 50 nm).

The textural properties of the catalysts are summarized in Table 2. Focusing on the catalysts of the first series (xNiSi SDI) it can be seen that the specific surface area (S_{BET}) and pore volume (PV) as well as the mean pore diameter (d_p) values gradually decrease with the increase of the nickel content. This is, of course, expected, but it is remarkable that the fall of the specific surface area is due to the reduction in the percentage weight of the support in the catalyst and cannot be attributed to the poor dispersion of Ni. For example, the drop of the specific surface area in the

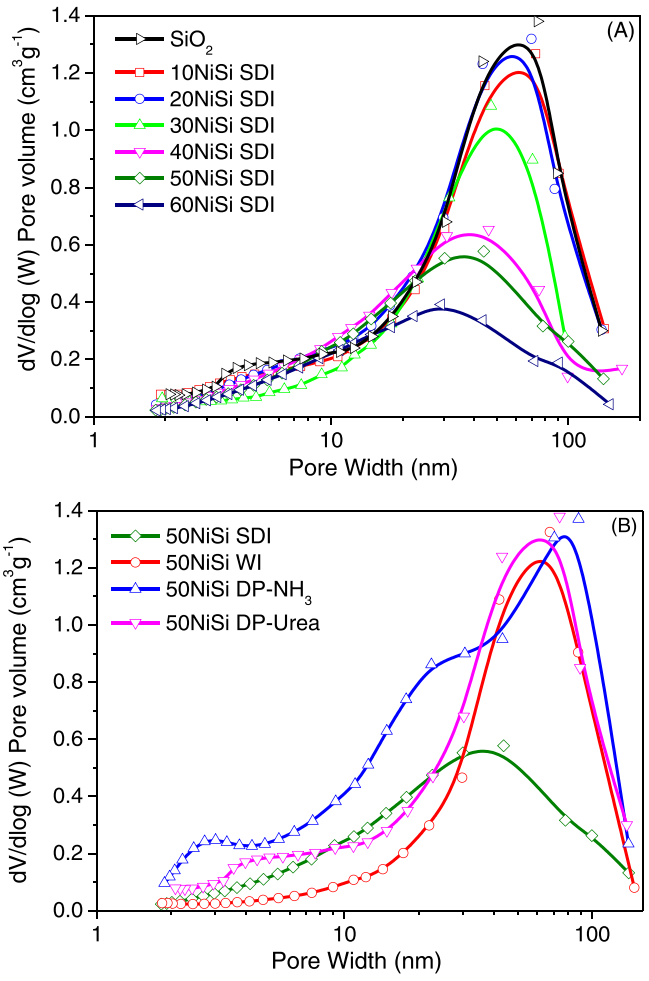

Fig. 1. Pore size distribution of (A) xNiSi SDI catalysts and (B) 50NiSi catalysts prepared by various methods.

50NiSi SDI catalyst is less than 50% relative to that of the bare support, although this catalyst contains 50% mass of support per gram of catalyst in comparison with the bare support. This is a first indication that even at very high Ni loadings, its dispersion on the surface of the support remains quite good, providing that the $Ni(en)_3(NO_3)_2$ has been used as the Ni precursor.

Concerning the active surface (determined through CO chemisorption), it increases with Ni loading up to 30 wt% and then it remains almost constant (in the range 30–50 wt%) or slightly decline at the higher nickel loading (60 wt%). These findings are in good agreement with the results obtained from XRD analysis (S^0_{Ni} values, Table 2).

Focusing on the second series of catalysts (50NiSi), it can be observed that the choice of the WI technique instead that of SDI results to a catalyst with slightly better characteristics (e.g. higher active surface). Moreover, the pore size distribution curve of this catalyst (Fig. 1(B)) is very similar to that of silica, indicating that nickel has been uniformly deposited on support surface without blocking mesopores. Noteworthy is the very high specific surface area (higher than that of the bare support) of the two catalysts prepared by a deposition-precipitation method. It appears that this technique leads to the formation of a new porous phase with increased pore volume in the region of the small mesopores (Fig. 1(B)). On the other hand, the active surface (determined through CO chemisorption) is quite low in these two catalysts.

XRD was performed to identify the crystal phases of the catalysts after activation (reduction) at 400 °C for 2.5 h. Inspection of Fig. 2(A) shows that silica used as support is mainly amorphous exhibiting a broad peak at around 2θ: 22° (JCPDS 39–1425). No other diffraction peaks of

Table 2
Textural and structural characteristics of the catalysts.[a].

Catalyst	S_{BET} (m^2g^{-1})	S^0_{Ni} (m^2g^{-1})	PV (cm^3 g^{-1})	d_p (nm)	MCS^0_{Ni} (nm)	CO chem. (μmole g^{-1})
SiO_2	192	–	0.97	21.6	–	–
10NiSi SDI	172	8.63	0.95	21.2	7.8	0.5
20NiSi SDI	162	14.18	0.93	21.8	9.5	28.1
30NiSi SDI	154	19.62	0.77	17.8	10.3	100.6
40NiSi SDI	139	19.52	0.61	16.8	13.8	103.4
50NiSi SDI	121	18.01	0.57	16.7	18.7	98.7
60NiSi SDI	101	16.49	0.40	14.2	24.5	92.4
50NiSi WI	124	25.13	0.72	22.1	13.4	109.7
50NiSi DP-NH_3	259	nd	1.10	18.0	nd	4.5
50NiSi DP-Urea	278	nd	1.23	16.4	nd	3.7

[a] S_{BET}: specific surface area calculated by BET equation; S^0_{Ni}: metallic nickel surface area per gram of catalyst, considering spherical shape Ni nanoparticles with diameter equal to their mean crystal size (MCS^0_{Ni}), calculated by XRD data and Scherrer equation; PV: pore volume in meso- and macropores; d_p: average pore size; nd: not detected; CO chem.: CO molecules chemisorbed on the metallic surface.

SiO_2 can be detected. This broad peak can also be observed at the diffraction pattern of 10NiSi SDI catalyst and to a lesser extent in the catalysts with higher nickel content up to the catalyst 40NiSi SDI. The peaks at 2θ: 44.38° [(111) d= 0.200 nm], 51.72° [(200), d= 0.177 nm] and 76.17° [(220), d= 0.126 nm] are indicative of supported metallic nickel nanocrystals (JCPDS 04–0850), while those at 2θ: 37.1° [(111) d= 0.241 nm], 43.1° [(200) d= 0.209 nm] and 62.5° [(220) d= 0.147 nm] can be attributed to the NiO phase (JCPDS 65–2901). It can be observed that the increase of Ni content leads to (a) increase of metallic nickel fraction at the expense of nickel oxide one, and (b) sharper and narrower diffraction peaks of metallic Ni, which indicates that the Ni crystal size increases. The Ni mean crystallite size (MCS^0_{Ni}) calculated by Scherrer equation is in good agreement with the aforementioned trend (Table 2). These observations are in accordance with the huge increase of CO chemisorption up to the 30NiSi SDI catalyst, and subsequent constancy at higher Ni loadings (Table 2).

Fig. 2(B) presents the XRD patterns of the activated catalysts synthesized by the four different preparation methods (successive dry impregnation, SDI; wet impregnation, WI; deposition precipitation with urea, DP-Urea; deposition precipitation with ammonia, DP-NH_3) containing 50 wt% Ni. The only phase detected for 50NiSi SDI is the metallic nickel, while for 50NiSi WI there is also the NiO phase. In contrast, none of these phases is detected by XRD analysis in the catalysts prepared by deposition – precipitation. This means that either such phases have not been formed or their dispersion is extremely high (crystal size lower than 4 nm). Instead, some new broad peaks at 2θ: 34.1°, 36.7° and 60.5° appeared at XRD patterns of the catalysts prepared by deposition precipitation. These peaks could be attributed to the nickel phyllosilicate species (PDF#49–1859) [50,62,63]. The above results are in accordance with the new porosity found from the N_2 adsorption measurements pointing to a new phase, as well as with the SEM image and the CO chemisorption measurements (Table 2), taking into account that CO molecules are chemisorbed only on the metallic surface.

SEM images of the 50NiSi catalysts prepared by various methods are presented in Fig. 3. They indicate the influence of preparation method

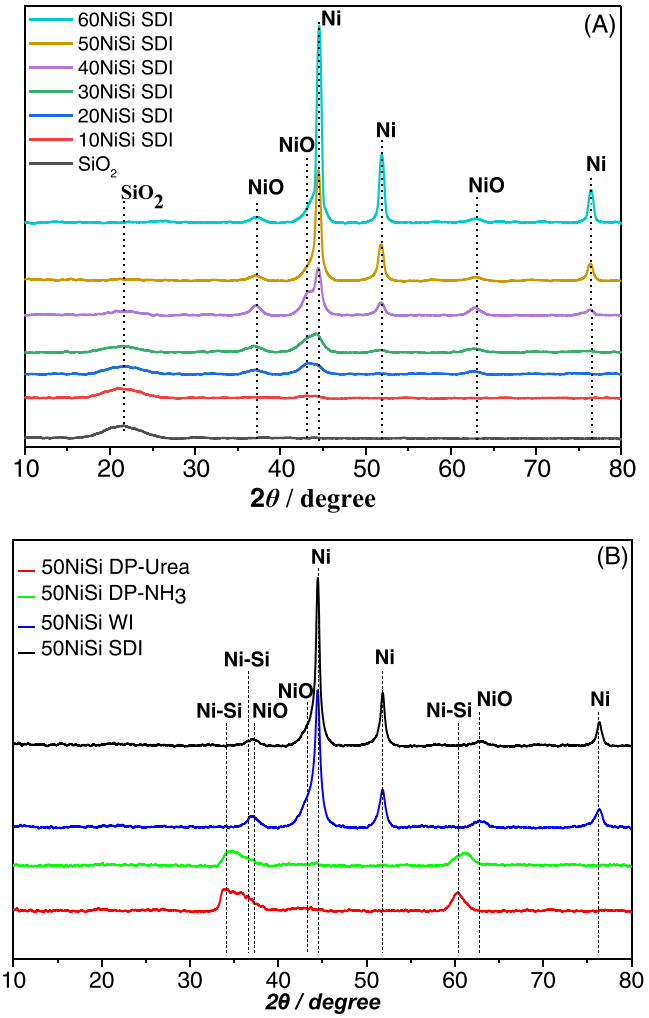

Fig. 2. XRD patterns of (A) SiO_2, 10 – 60NiSi SDI and (B) 50NiSi SDI, 50NiSi WI, 50NiSi DP-Urea, 50NiSi DP-NH_3.

on the catalyst morphology. The figure reveals that bulky nanoparticles are formed when SDI is applied. These become smaller in the WI catalyst (in agreement with the active surface results) and even smaller in the DP-NH_3 one. On the other hand, the catalyst morphology dramatically changed when the DP-Urea method has been followed. In this case, a flake – like morphology is observed. This morphology is common for supported nickel catalysts prepared by hydrothermal precipitation methods [64–68]. EDS analysis performed on these catalysts proved that the values of their Ni loading are too close to the nominal ones.

TEM images (Fig. 4) in agreement with XRD results reveal that significant changes of the catalysts structure take place, when different preparation methods are followed. Indeed, impregnation (SDI and WI) is responsible for the appearance of well-dispersed black spots (Ni nanoparticles) in TEM micrographs of the corresponding catalysts. These spots are smaller in the 50NiSi WI catalyst than those appearing in the 50NiSi SDI one, indicating a better dispersion of nickel in the first one. The DP-NH_3 method produced a catalyst with even smaller Ni nanoparticles in combination with some filamentous structures attributed to nickel phyllosilicate phase [69]. The latter phase becomes predominant in the 50NiSi DP-Urea catalyst.

The reduction profiles of the series of catalysts synthesized by SDI are depicted in Fig. 5(A). The reduction peak at about 200 °C is assigned to the free nickel oxide species weakly interacting with silica surface [70,71]. The overlapped peaks appearing in the temperature range 250 – 400 °C can be attributed to the reduction of nickel oxide species moderately interacting with the support surface [72] and the peak appearing at 450 °C is assigned to nickel oxide species strongly interacting with the silica support. The amount of H_2 consumed in any case is proportional to the catalyst's nickel content.

Fig. 5B illustrates the H_2 – TPR profiles of the 50NiSi samples prepared by SDI, WI, DP-NH_3 and DP-Urea method. Application of the impregnation methods (SDI and WI) led to identical reduction profiles, inducing, according to the previous discussion, the existence of three nickel oxide species, i.e. free-weakly interacting (reduced at 200 °C), moderately interacting (reduced at 250 – 400 °C) and strongly interacting (reduced at 450 °C) with silica surface. In contrast, adopting the deposition – precipitation methods a very broad reduction peak appears at temperatures higher than 250 °C. Supposing that kinetic effects are negligible in the TPR experiments, this broad peak indicates a plethora of nickel oxo – species with various interaction strengths with the silica support. The maximum of this peak appears at 465 °C in the case of 50NiSi DP-NH_3 sample, while it is shifted to 545 °C in the case of 50NiSi DP-Urea one. This means that stronger interactions between nickel oxo – species and silica are created when deposition – precipitation is applied for catalysts preparation. These interactions depend also on the preparation conditions (temperature and precipitation agent). The use of high temperature and urea as precipitating agent lead to stronger interactions than those created using ammonia as precipitating agent, at room temperature. In both cases, this H_2 consumption at high temperatures (400–650 °C) is attributed to the reduction of nickel phyllosilicate species [73–75]. This finding is in accordance with XRD results (Fig. 2(B)), which proved the formation of such species. The above results corroborate the literature finding that Ni ions in phyllosilicate are difficult to be reduced [50,63,73–76]. Moreover, it must be mentioned that even in these high temperatures, it seems that a significant portion of nickel has not been reduced, since the total hydrogen amount consumed upon the TPR experiments over the catalysts 50NiSi DP-NH_3 and 50NiSi DP-Urea is considerably lower that the corresponding one over the impregnation catalysts.

The acidic properties of silica and 10 – 60NiSi SDI catalysts were investigated using NH_3-TPD analysis (Fig. 6(A)). The corresponding desorption profiles indicate the presence of three types of acidic sites on the surfaces of these samples. Specifically, an NH_3 – desorption peak appearing at temperatures lower than 150 °C is indicative of very weak acid sites. A peak appearing in the range 150 – 250 °C is assigned to weak acid sites and that in the range 250 – 400 °C is attributed to acid sites of moderate acidity.

It is evident from Fig. 6(A) that the SiO_2 support exhibits very weak acid sites and few, if any, strong acid sites (>400 °C). The deposition of 10 wt% Ni on the SiO_2 surface provoked an increase of the total surface acidity in conjunction with the disappearance of the low temperature peak (<150 °C) and the appearance of three overlapped NH_3-desorption peaks in the range 150 – 400 °C corresponding to weak (majority) and moderate acid sites (few). It is obvious that the nickel phases deposited on the silica surface change the acidity–basicity of the samples concerning the weak, Bronsted type, sites. The increase in the total acidity is the result of a compromise between two opposite facts: the big increase of acidity due to the development of weak acid sites on the NiO supported nanoparticles [77] and the decrease of this type of acidity due to the coverage, by the nickel supported phases, of the less populated Si-OH weak acidic sites [78–81]. Upon increase of Ni loading to 20 wt% the total acidity remained constant but an increase of moderate acidity was detected. Further increase of Ni loading to 30 and 40 wt% is accompanied by an increase of the total acidity. The latter increase is mainly due to a reappearance of very weak acid sites on the surface of these catalysts. Further increase of the Ni loading did not change the total acidity but an increase of the population of moderate acid sites is evident mainly on 50NiSi SDI catalyst. Overall, it can be concluded that both weak and moderate acid sites are developed on the surface of the nickel containing catalysts, whereas strong acid sites are not detected (absence of TPD peaks at temperatures > 450 °C).

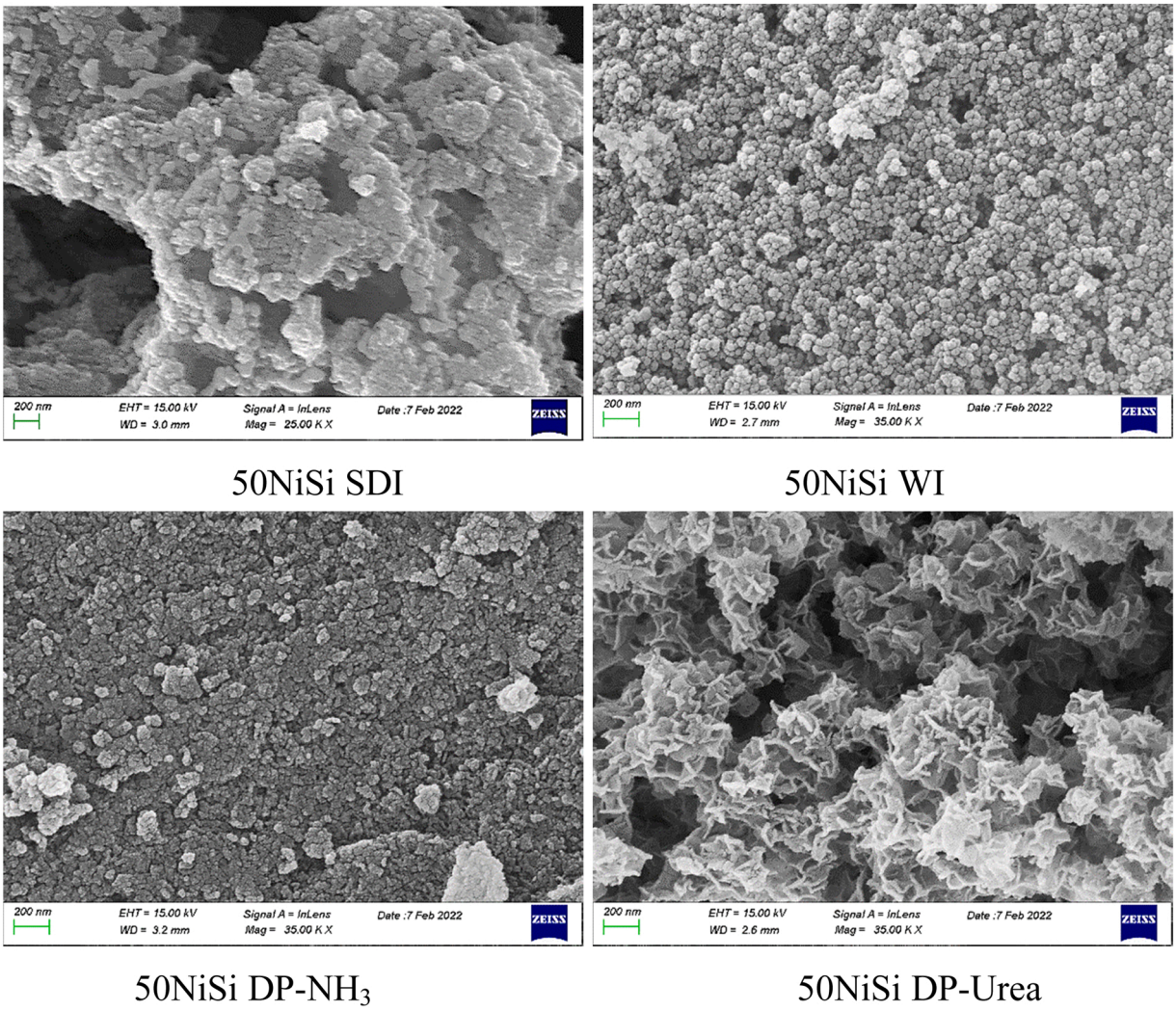

Fig. 3. SEM images of 50NiSi catalysts prepared by various methods.

Fig. 6(B) illustrates the NH_3 – TPD profiles of the 50NiSi catalysts prepared by various methods. The figure shows that when an impregnation method is used for catalyst synthesis, their total acidity is lower than that of the catalysts prepared by deposition – precipitation methods. Moreover, this low acidity is due to weak and moderate acid sites, while strong acid sites have been detected on the surface of the latter catalysts. One can observe that the 50NiSi DP-Urea catalyst exhibits the highest population of strong acid sites.

3.2. Catalysts' performance

A representative chromatogram of the liquid phase obtained upon the reaction of SDO of sunflower is given in Fig. 7. Similar chromatograms were obtained in the presence of both series of catalysts of the present study. As it can be seen, the main products were n-alkanes in the diesel range (n-C15 – n-C18), as well as palmitic and stearic acid, methyl, propyl, palmitic and stearic stearate and unreacted sunflower oil. Moreover, 2-decaoxy - ethyl stearate, distearine and 1-decaoctanol were detected in small quantities. The n-alkanes are the end products (green diesel) whereas all the other compounds are intermediate ones. The presence of all these products is consistent with the SDO mechanism, which is followed over the nickel non-sulphided catalysts and has been corroborated many times in the literature [53–56,61,82–85]. The first and very rapid step of this mechanism is the hydrogenation of the double bonds of the side chains of triglycerides. It follows the quite rapid step of gradual decomposition of the C-O bonds in the glycerol side. This leads, successively, to di– and mono– glycerides and then to propane with the simultaneous production of one molecule of fatty acid in each stage. The fatty acids, following a dehydration – decarbonylation (deH_2O – deCO) route, can be reduced to the corresponding aldehydes by water removal, which then are decarbonylated resulting again to n-alkanes with odd number of carbon atoms and CO. The intermediate aldehydes may, alternatively, further reduced and very rapidly equilibrated with the corresponding alcohols. These, then, are dehydrated to olefins, which are very rapidly hydrogenated to n-alkanes with even number of carbon atoms. Thus, the SDO through this route proceeds through dehydration (deH_2O). In parallel, the intermediate alcohols may react with the intermediate fatty acids, producing long chain esters. These may undergo SDO resulting to hydrocarbons.

Fig. 8 shows the evaluation of the catalysts of the first series (0–60 wt % Ni) at the maximum reaction time (9 h) of the SDO of sunflower oil. The wt% composition of the liquid reaction mixture, in total n-alkanes, total acids and total long esters, is illustrated. It can be seen that silica is almost inactive in the SDO of sunflower oil. It must be mentioned that the xNiSi catalysts are very active, exhibiting $>$ 90% conversion of the oil (not shown). In fact, conversion reaches 100% over the samples 50NiSi and 60NiSi. Moreover, as it can be observed, over all NiSi catalysts, considerable amounts of n-alkanes were produced. This corroborates the literature finding, that the supported nickel catalyzes all the steps of the SDO mechanism [53–56,61,82–85]. Another important

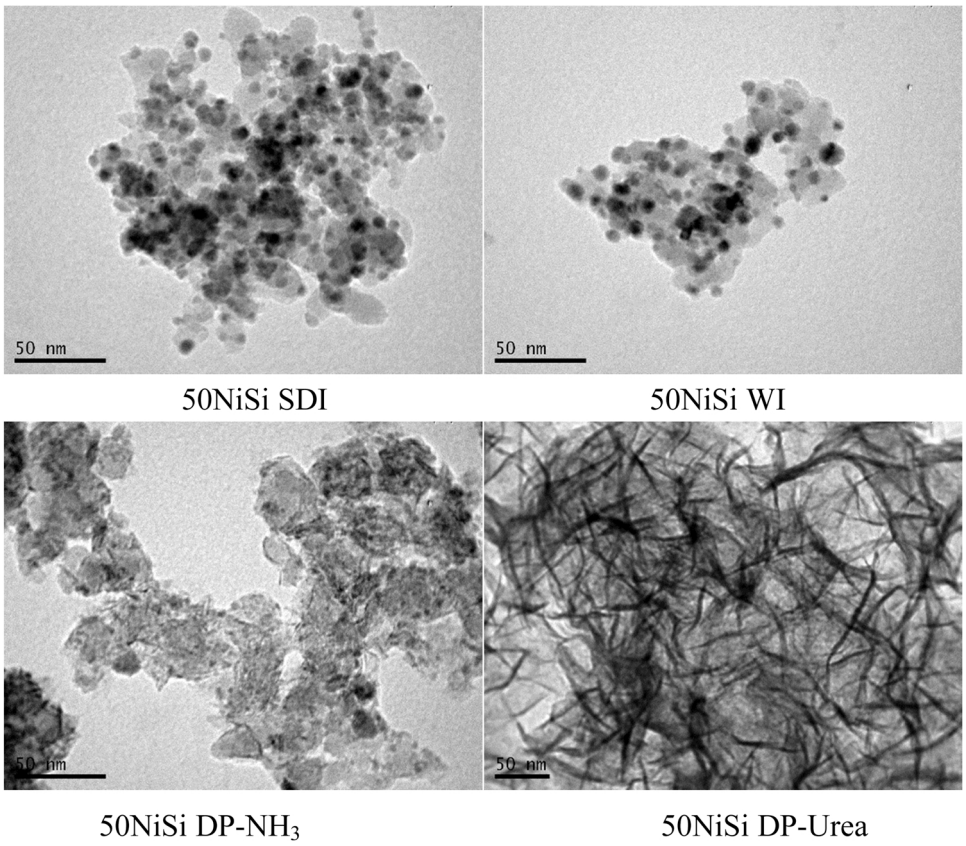

Fig. 4. TEM images of 50NiSi catalysts prepared by various methods.

observation is that the amount of n-alkanes in the liquid product (the most critical evaluation parameter from the practical point of view) follows a volcano curve. It monotonically increases with the Ni loading up to 50%, where it achieves a maximum, whereas at higher loading it decreases. Thus, the main finding of the study of the first series of catalysts is that the optimum Ni loading for the Ni/SiO_2 catalysts, concerning the SDO of sunflower oil to green diesel, is the 50 wt% Ni. This result is in agreement with the physicochemical characteristics of this catalyst, which showed high active surface of Ni (Table 2) in combination with high moderate acidity (Fig. 6(A)).

The kinetic data, concerning the SDO of sunflower oil over the most active catalyst of the first series (50NiSi SDI), are presented in Fig. 9. Similar kinetic curves were obtained in the presence of the other catalysts. It can be seen that the concentration of n-alkanes increases continually with the reaction time. On the contrary, both acids and esters pass through a maximum, indicating that they are intermediate molecules, as described previously and also reported in the literature [53–56,61,82–85]. Focusing on the n-alkanes produced (see Fig. 10), we can easily observe a selective production of n-alkanes with odd number of carbon atoms. If we recall the discussion about the SDO mechanism presented previously, we can conclude that SDO proceeds mainly via the decarbonylation of the intermediate aldehydes instead of the dehydration of the intermediate alcohols. This route is favored over the nickel supported catalysts [53–56,61,82–85].

Having found the most promising composition of the catalyst (50 wt % Ni), the second step was the examination of the effect of preparation methodology on the catalytic performance. The evaluation results are given in Fig. 11.

Although all catalysts achieve 100% conversion of the sunflower oil after 9 h of reaction, it can be concluded from Fig. 11 that the 50NiSi WI catalyst is the most effective one, since it achieves the higher yield to n-alkanes in the diesel range. This result is in agreement with the physicochemical characterization of the 50NiSi catalysts presented and discussed previously. In fact, the 50NiSi WI catalyst exhibited the higher active surface (metallic nickel surface) as determined by both CO chemisorption and XRD measurements (Table 2) and corroborated by SEM and TEM images. The adoption of the wet impregnation technique which uses a much larger volume impregnation solution (compared to the SDI) in combination with the $[Ni(en)_3]^{2+}$ as the precursor ion, which ensures a high dispersion of the Ni on silica by avoiding a direct precipitation of Ni in the impregnation solution upon drying, leads to a catalyst with very high dispersion of the active phase. Moreover, the 50NiSi WI catalyst exhibits high moderate acidity, which favors SDO of triglycerides towards hydrocarbons in the diesel range. On the other hand, the catalysts prepared by deposition-precipitation, exhibiting a very high surface area (Table 2) and a very high nickel dispersion (TEM), appear remarkable catalytic performance in the n-alkanes production (although lower than those of the impregnated catalysts). This unexpected behavior, on the basis of their low metallic Ni surface (Table 2), could be explained by an in-situ reduction of the very well dispersed nickel phyllosilicate phase (detected by XRD, SEM, TEM). In this phase, nickel is strongly interacting with silica, and thus not fully reducible even at very high temperatures upon H_2-TPR experiments. However, under strong reductive conditions (40 bar H_2 pressure adopted during SDO of sunflower oil), a part of nickel contained in nickel phyllosilicate phase could be reduced to metallic Ni, increasing thus the metallic surface area and consequently the catalytic performance. On the other hand, the strong acidity of the DP catalysts (Fig. 6B) is expected to have a negative effect on their performance. Overall, it seems that the key factor in the catalytic performance concerning the production of n-alkanes is the combination of a high metallic nickel surface with an intermediate acidity. The same conclusion was drawn from a recent study concerning the SDO of triglycerides over nickel catalysts supported on palygorskite, a natural mineral containing silicate units [56].

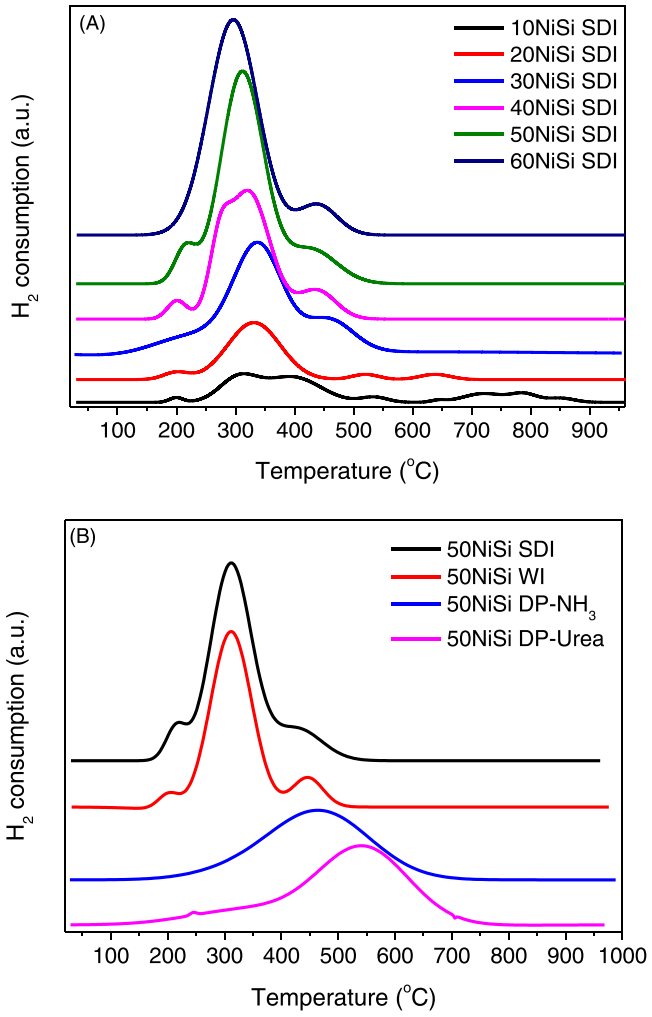

Fig. 5. H_2 – TPR profiles of (A) 10 – 60NiSi SDI samples and (B) 50NiSi samples prepared by various methods.

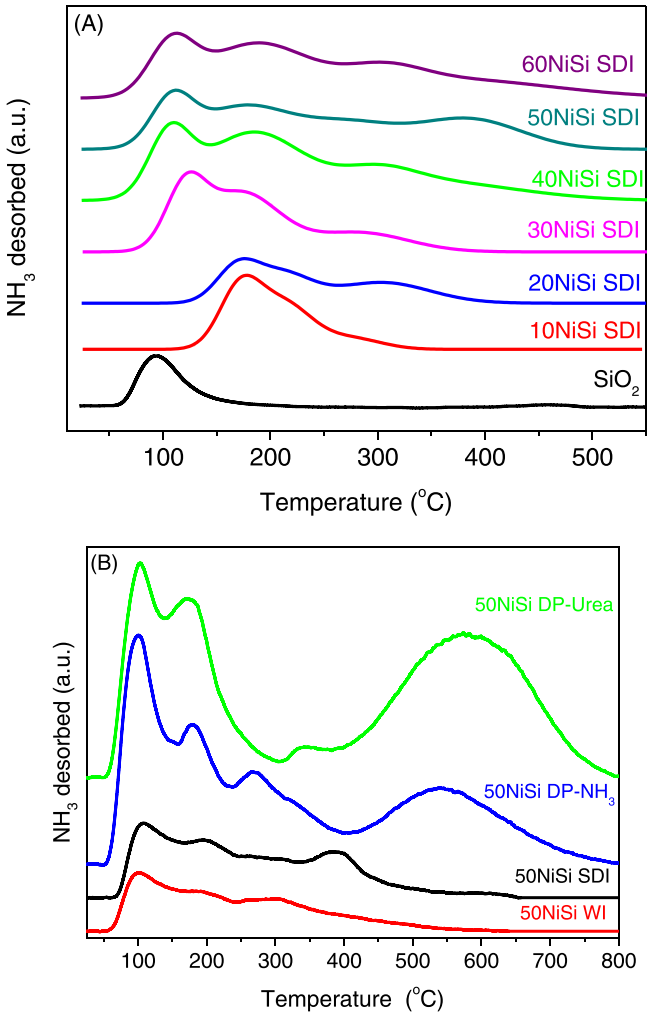

Fig. 6. NH_3 – TPD profiles of (A) SiO_2 and 10 – 60NiSi SDI catalysts and (B) 50NiSi catalysts prepared by various methods.

Finally, it must be mentioned that if one takes into account both the very large amount of oil (100 mL) in proportion to that of the catalyst (1 g) and the conditions of the catalytic tests characterized by the lack of solvent, the concentration of n-alkanes in the liquid product is very high [16]. This shows that silica is a promising carrier for developing nickel supported catalysts in order to be used for the production of green diesel. This high performance of the catalysts is attributed to the high dispersion ability of silica in conjunction with the synthesis method adopted for dispersing nickel on its surface, namely wet impregnation using $[Ni(en)_3]^{2+}$ as the precursor nickel ion.

4. Conclusions

The main conclusions of the present study are the following:

- The optimum Ni loading for the Ni/SiO_2 catalysts, prepared by SDI, concerning the transformation of sunflower oil to green diesel is the 50 wt%, since this catalyst exhibits the best combination of high active nickel surface and moderate acidity.
- Impregnation of silica with the $[Ni(en)_3]^{2+}$, as the precursor ion, ensures a high dispersion of the Ni. This is more pronounced when the Wet Impregnation has been used instead of the Successive Dry Impregnation technique, resulting thus to the most efficient catalyst (50NiSi WI).
- The catalysts prepared by Deposition-Precipitation, although exhibiting a very high specific surface area and a very high nickel dispersion, they did not appear more effective in the green diesel production. This is due to the formation of a very well dispersed nickel phyllosilicate phase, in which nickel was strongly interactive with silica, thus not fully reducible and consequently inactive in the selective deoxygenation of sunflower oil.
- The catalysts exhibited very good performance in the transformation of sunflower oil into green diesel, taking into account both the very large amount of oil (100 mL) in proportion to that of the catalyst (1 g) and the solvent free conditions of the catalytic tests. The above indicated that silica is a promising carrier for developing nickel supported catalysts to be used in the production of green diesel.

CRediT authorship contribution statement

John Zafeiropoulos: Resources, Methodology, Investigation. **George Petropoulos:** Methodology, Investigation, Validation. **Eleana Kordouli:** Formal analysis, Data curation, Visualization. **Christos Kordulis:** Conceptualization, Writing – original draft. **Alexis Lycourghiotis:** Conceptualization, Writing– review & editing. **Kyriakos Bourikas:** Writing – review & editing, Supervision, Project administration.

Declaration of Competing Interest

The authors declare that they have no known competing financial

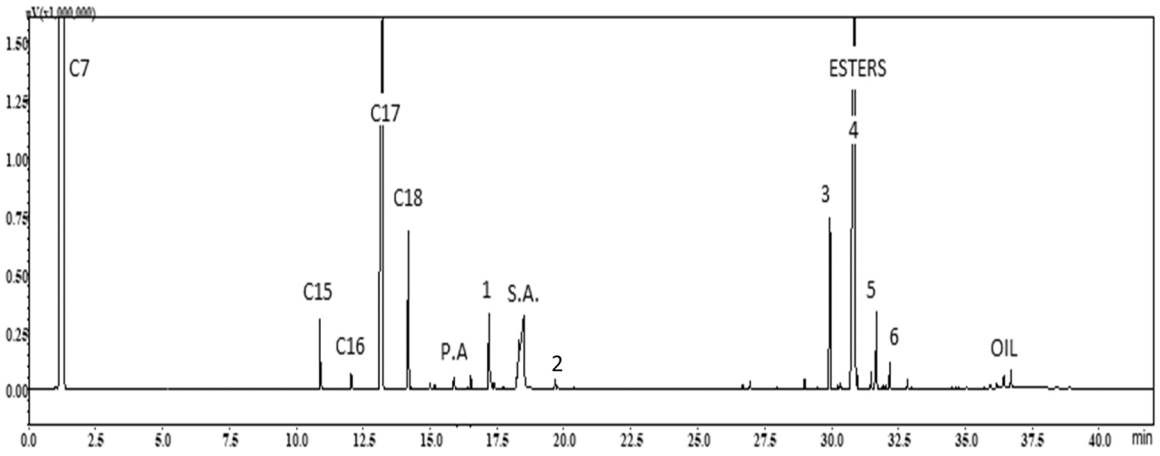

Fig. 7. Typical chromatogram of the liquid reaction mixture obtained upon the SDO of sunflower oil over the 50NiSi SDI catalyst, after 5 h (C7: heptane used as internal standard, C15-C18: n-alkanes with corresponding number of carbon atoms, P.A.: palmitic acid, S.A.: stearic acid, 1: 1-octadecanol, 2: propyl stearate, 3: palmityl stearate, 4: stearyl stearate, 5: 2-(octadecyloxy) ethyl stearate, 6: distearine).

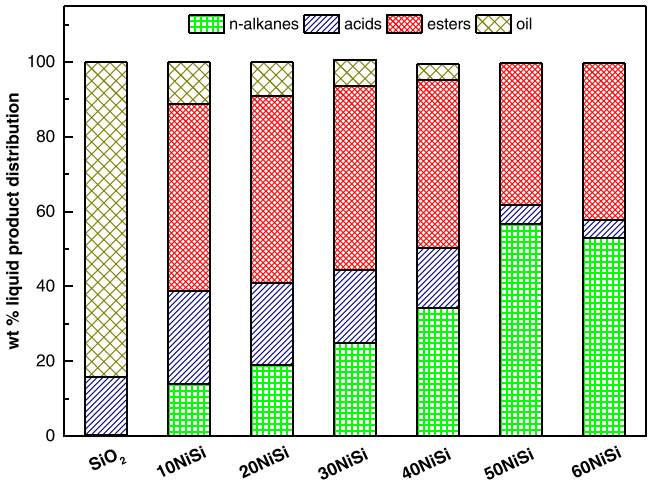

Fig. 8. Liquid phase composition of the reaction mixture after 9 h, over the catalysts xNiSi SDI.

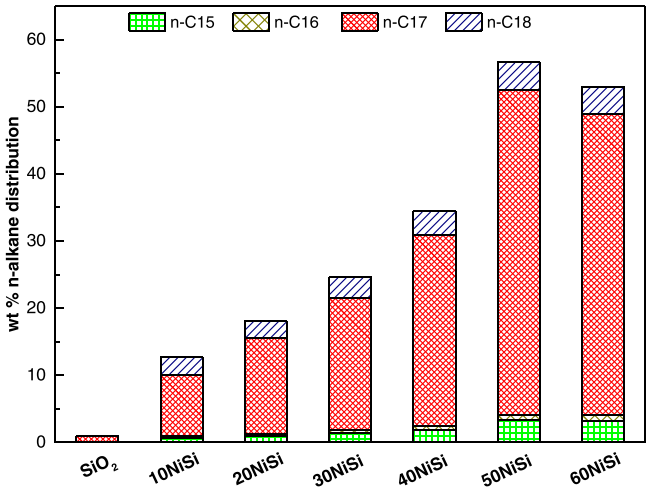

Fig. 10. Hydrocarbons composition of the liquid reaction mixture after 9 h, over the xNiSi SDI catalysts.

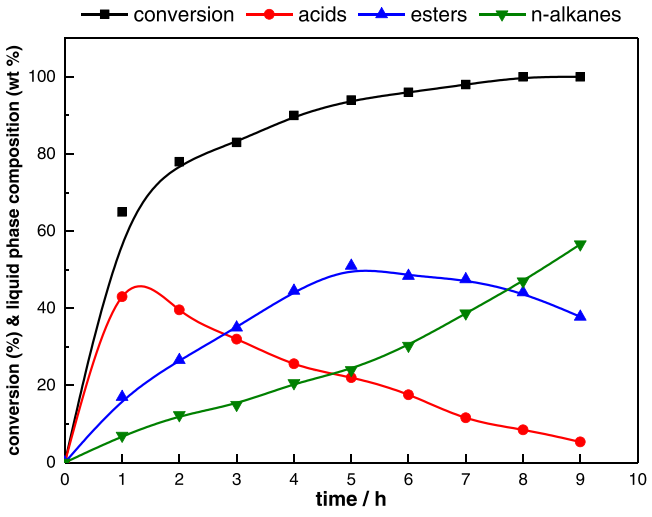

Fig. 9. Kinetics of SDO of sunflower oil over the 50NiSi SDI catalyst.

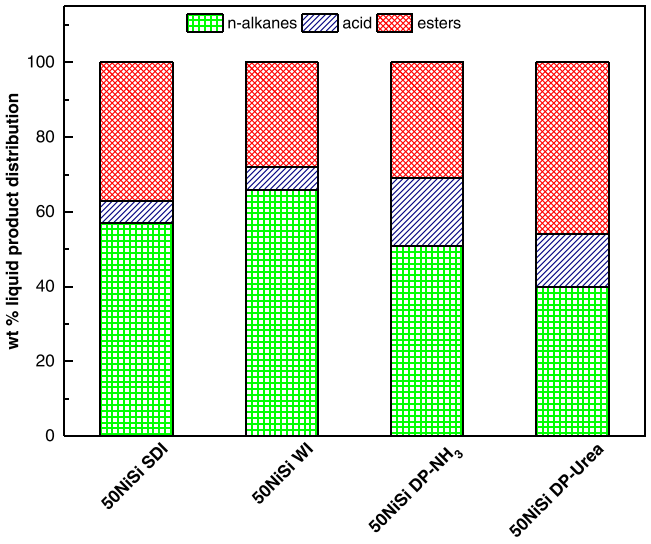

Fig. 11. Liquid phase composition of the reaction mixture after 9 h, over the 50NiSi catalysts.

interests or personal relationships that could have appeared to influence the work reported in this paper.

Data Availability

Data will be made available on request.

Acknowledgment

Dr. M. Kollia is acknowledged for her contribution in recording the TEM images of the catalysts at the laboratory of Electron Microscopy and Microanalysis of the University of Patras. Dr. V. Dracopoulos (FORTH/ICE-HT) is also acknowledged for his contribution in recording the SEM images.

References

[1] N. Armaroli, V. Balzani, Angew. Chem. Int. Ed. 46 (2007) 52–66.
[2] S.L. Douvartzides, N.D. Charisiou, K.N. Papageridis, M.A. Goula, Energies 12 (2019) 809.
[3] A. Alegria, J. Cuellar, Appl. Catal. B 179 (2015) 530.
[4] J. Rodríguez-Fernández, J.J. Hernández, A. Calle-Asensio, Á. Ramos, J. Barba, Energies 12 (2019) 2034.
[5] D. Kubička, I. Kubičková, J. Čejka, Catal. Rev. 55 (2013) 1–78.
[6] X. Yao, T.J. Strathmann, Y. Li, L.E. Cronmiller, H. Ma, J. Zhang, Green. Chem. 23 (2021) 1114–1129.
[7] H.I. Mahdi, A. Bazargan, G. McKay, N.I.W. Azelee, L. Meili, Chem. Eng. Res. Des. 174 (2021) 158–187.
[8] C. Kordulis, K. Bourikas, M. Gousi, E. Kordouli, A. Lycourghiotis, Appl. Catal. B 181 (2016) 156–196.
[9] S. Bezergianni, A. Dimitriadis, D. Karonis, Fuel 136 (2014) 366–373.
[10] T.N. Kalnes, K.P. Koers, T. Marker, D.R. Shonnard, Sustain. Energy 28 (2009) 111–120.
[11] I. Simakova, O. Simakova, P. Mäki-Arvela, D.Yu Murzin, Catal. Today 150 (2010) 28–31.
[12] F.P. de Sousa, C.C. Cardoso, V.M.D. Pasa, Fuel Process. Technol. 143 (2016) 35–42.
[13] L. Yang, M.A. Carreon, ACS Appl. Mater. Interfaces 9 (2017) 31993–32000.
[14] K. Kon, T. Toyao, W. Onodera, S.M. a H. Siddiki, K. Shimizu, ChemCatChem 9 (2017) 2822–2827.
[15] S. Janampelli, S. Darbha, Energy Fuels 32 (2018) 12630–12643.
[16] A.E. Coumans, E.J.M. Hensen, Appl. Catal. B 201 (2017) 290–301.
[17] P. Arora, H. Ojagh, J. Woo, E. Lind Grennfelt, L. Olsson, D. Creaser, Appl. Catal. B 227 (2018) 240–251.
[18] E.N. Vlasova, G.A. Bukhtiyarova, I.V. Deliy, P.V. Aleksandrov, A.A. Porsin, M. A. Panafidin, E.Yu Gerasimov, V.I. Bukhtiyarov, Catal. Today 357 (2020) 526–533.
[19] X. Li, X. Luo, Y. Jin, J. Li, H. Zhang, A. Zhang, J. Xie, Renew. Sustain. Energy Rev. 82 (2018) 3762–3797.
[20] A. Srifa, N. Viriya-empikul, S. Assabumrungrat, K. Faungnawakij, Catal. Sci. Technol. 5 (2015) 3693–3705.
[21] S. Chen, G. Zhou, C. Miao, Renew. Sustain. Energy Rev. 101 (2019) 568–589.
[22] H. Xin, H. Yang, X. Lei, X. Du, K. Zhou, D. Li, C. Hu, Ind. Eng. Chem. Res. 59 (2020) 17373–17386.
[23] X. Niu, X. Li, G. Yuan, F. Feng, M. Wang, X. Zhang, Q. Wang, Ind. Eng. Chem. Res. 59 (2020) 8601–8611.
[24] H. Liu, J. Han, Q. Huang, H. Shen, L. Lei, Z. Huang, Z. Zhang, Z.K. Zhao, F. Wang, Ind. Eng. Chem. Res. 59 (2020) 17440–17450.
[25] W.N.A.W. Khalit, N. Asikin-Mijan, T.S. Marliza, M.S. Gamal, M.R. Shamsuddin, M. I. Saiman, Y.H. Taufiq-Yap, Biomass-.-. Bioenergy 154 (2021), 106248.
[26] B. Veriansyah, J.Y. Han, S.K. Kim, S.-A. Hong, Y.J. Kim, J.S. Lim, Y.-W. Shu, S.-G. Oh, J. Kim, Fuel 94 (2012) 578–585.
[27] D. Kubička, L. Kaluža, Appl. Catal. A 372 (2010) 199–208.
[28] H. Shi, J. Chen, Y. Yang, S. Tian, Fuel Proc. Technol. 118 (2014) 161–170.
[29] B. Peng, X. Yuan, C. Zhao, J.A. Lercher, J. Am. Chem. Soc. 134 (2012) 9400–9405.
[30] B. Peng, C. Zhao, S. Kasakov, S. Foraita, J.A. Lercher, Chem. Eur. J. 19 (2013) 4732–4741.
[31] H.L. Zuo, Q.Y. Liu, T.J. Wang, N. Shi, J.G. Liu, L.L. Ma, J. Fuel, Chem. Technol. 40 (2012) 1067–1073.
[32] L. Liu, Y. Liu, X. Gao, R. Zhang, Y. Zhai, J. Fuel, Chem. Technol. 45 (2017) 932–938.
[33] R. Zarchin, M. Rabaev, R. Vidruk-Nehemya, M.V. Landau, M. Herskowitz, Fuel 139 (2015) 684–691.
[34] Y. Yang, C. Ochoa-Hernández, P. Pizarro, V.A. de la Peña O'Shea, J.M. Coronado, D.P. Serrano, Fuel 144 (2015) 60–70.
[35] M.F. Kamaruzaman, Y.H. Taufiq-Yap, D. Derawi, Biomass Bioenergy 134 (2020), 105476.
[36] C. Ochoa-Hernández, Y. Yang, P. Pizarro, V.A. de la Peña O'Shea, J.M. Coronado, D.P. Serrano, Catal. Today 210 (2013) 81–88.
[37] C. Liu, H. Yang, Z. Jing, K. Xi, C. Qiao, J. Fuel, Chem. Technol. 44 (2016) 1211–1216.
[38] Q. Liu, H. Zuo, Q. Zhang, T. Wang, L. Ma, Chin. J. Catal. 35 (2014) 748–756.
[39] H. Jeong, M. Shin, B. Jeong, J.H. Jang, G.B. Han, Y.-W. Suh, J. Ind. Eng. Chem. 83 (2020) 189–199.
[40] A.J. van Dillen, R.J.A.M. Terörde, D.J. Lensveld, J.W. Geus, K.P. de Jong, J. Catal. 216 (2003) 257–264.
[41] L.-Y. Wang, G.-Q. Wu, D.G. Evans, Mater. Chem. Phys. 104 (2007) 133–140.
[42] S. Boujday, J.-F. Lambert, M. Che, J. Phys. Chem. B 107 (2003) 651–654.
[43] L. Espinosa-Alonso, K.P. de Jong, B.M. Weckhuysen, J. Phys. Chem. C. 112 (2008) 7201–7209.
[44] K.-Q. Sun, E. Marceau, M. Che, Phys. Chem. Chem. Phys. 8 (2006) 1731–1738.
[45] D. Valencia, L. Peña, V.H. Uc, I. García-Cruz, Appl. Catal. A 475 (2014) 134–139.
[46] J.Y. Carriat, M. Che, M. Kermarec, M. Verdaguer, A. Michalowicz, J. Am. Chem. Soc. 120 (1998) 2059–2070.
[47] F. Negrier, E. Marceau, M. Che, D. de Caro, Comptes Rendus Chim. 6 (2003) 231.
[48] F. Negrier, E. Marceau, M. Che, J.-M. Giraudon, L. Gengembre, A. Lofberg, Catal. Lett. 124 (2008) 18.
[49] E. Marceau, A. Löfberg, J.-M. Giraudon, F. Negrier, M. Che, L. Leclercq, Appl. Catal. A 362 (2009) 34.
[50] P. Burattin, M. Che, C. Louis, J. Phys. Chem. B 102 (1998) 2722.
[51] P. Munnik, P.E. de Jongh, K.P. de Jong, Chem. Rev. 115 (2015) 6687–6718.
[52] P. Mäki-Arvela, D.Yu Murzin, Appl. Catal. A 451 (2013) 251–281.
[53] M. Gousi, C. Andriopoulou, K. Bourikas, S. Ladas, M. Sotiriou, C. Kordulis, A. Lycourghiotis, Appl. Catal. A 536 (2017) 45–56.
[54] I. Nikolopoulos, G. Kogkos, E. Kordouli, K. Bourikas, C. Kordulis, A. Lycourghiotis, Mol. Catal. 482 (2020), 110697.
[55] G. Zafeiropoulos, N. Nikolopoulos, E. Kordouli, L. Sygellou, K. Bourikas, C. Kordulis, A. Lycourghiotis, Catalysts 9 (2019) 210.
[56] S. Lycourghiotis, E. Kordouli, L. Sygellou, K. Bourikas, C. Kordulis, Appl. Catal. B 259 (2019), 118059.
[57] X. Zhao, L. Wei, S. Cheng, J. Julson, G. Anderson, K. Muthukumarappan, C. Qiu, J. Renew. Sustain. Energy 8 (2016), 013109.
[58] P.B. Weisz, W.O. Haag, P.G. Rodewald, Science 206 (1979) 57–58.
[59] G. Knothe, Prog. Energy Combust. Sci. 36 (2010) 364–373.
[60] S.B. Glisic, J.M. Pajnik, A.M. Orlovic, Appl. Energy 170 (2016) 176–185.
[61] E. Kordouli, L. Sygellou, C. Kordulis, K. Bourikas, A. Lycourghiotis, Appl. Catal. B 209 (2017) 12–22.
[62] L. Liao, L. Chen, R.-P. Ye, X. Tang, J. Liu, Chem. Asian J. 16 (2021) 678–689.
[63] P. Burattin, M. Che, C. Louis, J. Phys. Chem. B 101 (1997) 7060.
[64] E. Kordouli, B. Pawelec, K. Bourikas, C. Kordulis, J.L.G. Fierro, A. Lycourghiotis, Appl. Catal. B 229 (2018) 139–154.
[65] R. Miao, X. Yu, W. Zeng, Mater. Lett. 173 (2016) 107–110.
[66] R. Miao, W. Zeng, Q. Gao, Appl. Surf. Sci. 384 (2016) 304–310.
[67] J. Wang, W. Zeng, Z. Wang, Ceram. Int. 42 (2016) 4567–4573.
[68] X. Liu, X. Wang, X. Yuan, W. Dong, F. Huang, J. Mater. Chem. A 4 (2016) 167–172.
[69] A. Rodriguez-Gomez, A. Caballero, ChemNanoMat 3 (2017) 94–97.
[70] H. Du, X. Ma, M. Jiang, P. Yan, Y. Zhao, Z. Conrad Zhang, Catal. Today 365 (2021) 265–273.
[71] X. Kong, Y. Zhu, H. Zheng, X. Li, Y. Zhu, Y.-W. Li, ACS Catal. 5 (2015) 5914–5920.
[72] F. Yang, D. Liu, Y. Zhao, H. Wang, J. Han, Q. Ge, X. Zhu, ACS Catal. 8 (2018) 1672–1682.
[73] M. Song, Z. Huang, B. Chen, S. Liu, S. Ullah, D. Cai, G. Zhan, J. CO_2 Util. 52 (2021), 101674.
[74] B.-H. Chen, Z.-S. Chao, H. He, C. Huang, Y.-J. Liu, W.-J. Yi, X.-L. Wei, J.-F. An, Dalton Trans. 45 (2016) 2720–2739.
[75] E. Soghrati, T.K.C. Ong, C.K. Poh, S. Kawi, A. Borgna, Appl. Catal. B 235 (2018) 130–142.
[76] P. Burattin, M. Che, C. Louis, J. Phys. Chem. B 104 (2000) 10482.
[77] T. Mahmood, M.T. Saddique, A. Naeem, P. Westerhoff, S. Mustafa, A. Alum, Ind. Eng. Chem. Res. 50 (2011) 10017–10023.
[78] M. Pfeiffer-Laplaud, D. Costa, F. Tielens, M.-P. Gaigeot, M. Sulpizi, J. Phys. Chem. C. 119 (2015) 27354–27362.
[79] M. Kosmulski, Adv. Colloid Interface Sci. 251 (2018) 115–138.
[80] M. Sulpizi, M.-P. Gaigeot, M. Sprik, J. Chem. Theory Comput. 8 (2012) 1037–1047.
[81] A.H. Jalil, U. Pyell, J. Phys. Chem. C 122 (2018) 4437–4453.
[82] S. Lycourghiotis, E. Kordouli, J. Zafeiropoulos, C. Kordulis, K. Bourikas, Molecules 27 (2022) 643.
[83] C. Papadopoulos, E. Kordouli, L. Sygellou, K. Bourikas, C. Kordulis, A. Lycourghiotis, Fuel Process. Technol. 217 (2021), 106820.
[84] M. Gousi, E. Kordouli, K. Bourikas, E. Simianakis, S. Ladas, G.D. Panagiotou, C. Kordulis, A. Lycourghiotis, Catal. Today 355 (2020) 903–909.
[85] M. Gousi, E. Kordouli, K. Bourikas, E. Symianakis, S. Ladas, C. Kordulis, A. Lycourghiotis, Energies 13 (2020) 3707.